SAARLAND UNIVERSITY

MASTER'S THESIS IN COMPUTER SCIENCE

Fabrication of objects with controlled deformation behaviour using tetrakaidecahedron cells

---

Author:
Ildar Gilmutdinov

Supervisor:
Dr. Piotr Didyk

Advisor:
Michal Piovarci

Reviewers:
Dr. Piotr Didyk
Prof. Dr. Jürgen Steimle

A thesis submitted in fulfillment of the requirements for the degree of Master of Computer Science

in the

Perception, Display and Fabrication
Faculty of Natural Sciences and Technology I

September 28, 2017

Erklärung

Ich erkläre hiermit, dass ich die vorliegende Arbeit selbständig verfasst und keine anderen als die angegebenen Quellen und Hilfsmittel verwendet habe.

Statement

I hereby confirm that I have written this thesis on my own and that I have not used any other media or materials than the ones referred to in this thesis

Einverständniserklärung

Ich bin damit einverstanden, dass meine (bestandene) Arbeit in beiden Versionen in die Bibliothek der Informatik aufgenommen und damit veröffentlicht wird.

Declaration of Consent

I agree to make both versions of my thesis (with a passing grade) accessible to the public by having them added to the library of the Computer Science Department.

Saarbrücken, _____ _____

(Datum/Date) (Unterschrift/Signature)

Abstract

One of the main needs of a 3D printer user is to control stiffness of the printed objects. Despite of the rapid growth of 3D printing industry, modern devices are still limited in the available material gamut. Several approaches were proposed in order to overcome this limitation. Among them there is a family of methods that use microstructures that allow to achieve a wide range of material properties. However, they possess disadvantages such as discretization at transition margin between regions of different stiffness and high possibility of the underlying microstructure to be broken due to localized stresses. In this work, we wanted to explore how to extend one of the methods to achieve a gradual transition change and make printed objects more durable . Using the theory developed in material science we propose to use the tetrakaidecahedron cell with one of the highest theoretical durability values. We derived the model to relate density of a cell grid and its mechanical properties. Knowing the target density, we can optimize cell grid geometry according to the desired elasticity thus achieving a continuous heterogenous distribution of properties within the object. To enable an intuitive way of designing objects with varying elastic properties, we allow user to specify how object should deform under a given force. This information is later used in an optimization procedure to compute the distribution of elastic properties within the object.

Contents

List of Figures

List of Tables

Chapter 1

Introduction

With a growth and development of 3D printing industry, it became possible to fabricate objects of various scale, complexity and precision. On one hand, industry can achieve highly flexible mass-production process by quickly readjusting setup of the machines. On the other hand, artists can use 3D printing for rapid prototyping to give additional dimension of perception in exploration of their work. There are many fabrication technologies, such as fused deposition modeling, where the tool drops filament at certain positions or selective laser sintering and digital light processing, which are based on solidification of polymers under light exposure. These technologies, commonly referred as additive manufacturing, ganed wide recognition. Though they differ in their approaches, they are quite similar in the challenges users meet by working with them.

One of them are fabricability constraints. Not every shape can be printed. If overhead angle is too big, the model will collapse and fall. Another significant problem is a limited material gamut. In most cases, only one material per printing process is available. This implies constraints not only on visual aspects, such as color, but also on the mechanical properties that can be reproduced. Next problem to be considered is the computation effort required to procces model mesh.

These challenges were addressed in several works. One of the first to overcome limited material gamut was carried out in [Bickel et al., 2010]. There, new materials were obtained by stacking layers of base materials, available for the printing device, and the combination of layers with desired deformation behaviour being found through discrete optimization process.

In contrast to [Bickel et al., 2010], other works [Panetta et al., 2015, Schumacher et al., 2015, Martínez, Dumas, and Lefebvre, 2016] were concentrated on the use of microstructures. Using homogenization theory [Allaire, 2002], one can obtain the coarse-level elastic properties of the tiled object, knowing properties of the unit tile. Complementary problem, i.e. in finding a tile that could yield a desired behaviour on macrolevel, was approached by [Bendsoe and Sigmund, 2004]. [Panetta et al., 2015] used it to generate families of metamaterials, each covering some part of possible material space. Despite of the advantages, such as flexible control and reduced material usage, new challenges arise: connectivity and continuity problem. They appear due to the fact that the shape of each structure is individual and not any two tiles can be connected with each other. [Panetta et al., 2015] used to generate families of microstructures by specific parametrization of nodes and struts, which allowed to average neighboring cells to connect them. [Schumacher et al., 2015] used to populate space of possible microstructures by continuously interpolating structures that are close to each other in terms of elastic properties. Having several different candidates for a single material property allowed to formulate connectivity problem as an assignment problem, minimizing discrepancies between neighboring cells.

Solving an optimization problem is often a costly computational task. [Martínez, Dumas, and Lefebvre, 2016] proposed to use a Voronoi Diagram (VD) as a basic microstructure, where elastic behaviour is controlled through a polynomial relating VD properties with elastic properties. Though this method in some way approaches continuity problem and there is no problem with connectivity by construction, it has issues with fabricability. Firstly, some of the edges can be overhanged. They can fail to be printed and due to complex truss structure, it can cause the whole structure to collapse. On the other hand, the structure can be generated in such a way that load during interaction is distributed unevenly and slight press can damage the object.

In this thesis we address the challenges discussed above, yet trying to avoid arising issues. Our work is based on generation of microstructures using Voronoi Diagram similarly to [Martínez, Dumas, and Lefebvre, 2016]. In contrast to them, we are looking for regular structures rather than stochastic ones. We generate open-cell foam, where edges of each cell form a specific polyhedron called *tetrakaidecahedron*, or a *Kelvin cell* in material science. This structure exhibits lower value of isotropy than an irregular one, but posseses higher durability.

In Chapter Two, we give a description of mechanical models developed in material science that allow to relate microstructure's geometry and the mechanical properties it will have on macroscale. Also, we will try to derive an empirical model from the samples that we fabricate and compare it to analytical ones.

In Chapter Three, we address the problem of achieving a continuous heterogenous distribution of elastic properties within the object. Briefly, idea of the method lies in imposing a cubical grid over the mesh and deform it in a specific way. Elasticity of the single tetrakaidecahedron cell mainly depends on its size. Thus, by controlling spatial variation of the sizes within the grid, we can achieve a connected structure meeting prescribed requirements with smooth transitions. The process of derivation of elasticity from the description of deformation behaviour is performed by the method described in [Xu et al., 2015].

The results of the conducted experiments and simulations are presented in Chapter 4.

As the outline, our main contributions are:

- We experimentally analyzed the use of a Kelvin cell as a more durable alternative to a Random Voronoi Foam
- We explored existing material science models to relate the size of a unit Kelvin cell structure with its stiffness and validated them on collected measurements
- We developed a framework for computation of an object tiling to achieve a heterogenous deformation behaviour distribution

Chapter 2

Homogenous foam

This chapter is devoted to homogenous foams in a sense of its geometry and properties within one body. Firstly, we introduce fundamental concepts of material mechanics in order to make the reader familiar with terms that we use. Next, we will give a description of tetrakaidecahedron (Kelvin) structure and discuss approaches to predict its mechanical properties. Finally, we will describe the process of the actual fabrication of the foams.

2.1 Background on material mechanics

The simplest analysis tool to assess basic material properteis is a force-displacement curve. It depicts how much force was applied to an object when it was undergoing a certain deformation. However, these quantities depend on the object size. In order to avoid it, we use quantitites that characterize intrinsic properties of a material: *stress* σ and *strain* ϵ. They correspond to force and displacement normalized by interaction area and sample size:

$$\sigma = \frac{F}{A}, \tag{2.1}$$

$$\epsilon = \frac{d}{L}, \tag{2.2}$$

where F is a measured force and A is an area of load, d is a measured displacement and L is the size of sample in the direction of applied force. Using these quantities, we can define a *stress-strain curve* as a size independent alternative to the force-displacement curve:

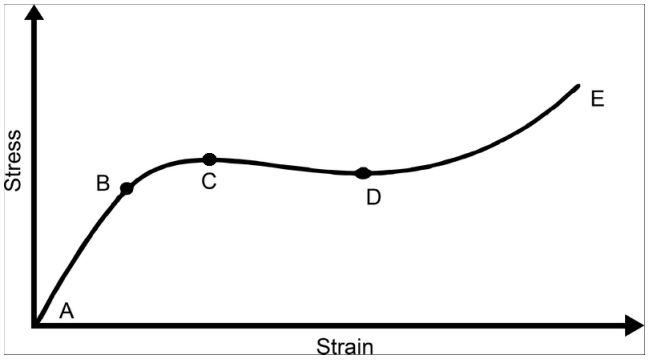

FIGURE 2.1: Stress-strain curve

The curve (2.1) depicts how much stress the material exerts, when it undergoes certain deformation. One can see three regions on this curve : AB - rising, BCD - plateau and then again rising DE. We are interested in the first region. It describes

object's elastic behaviour, which means that the object will return to its original state after endured deformation. Incline of this line defines central quantity that we will use - the *Young's modulus* E

$$E = \frac{\sigma}{\epsilon} \tag{2.3}$$

The curve region after the first peak describes object's plastic behaviour. At this point (the point C in the Fig. 2.1), the object will undergo irreversible deformations. Using Young's modulus for a material description means simplification of the material's behaviour to a linear one. There are many other models that capture non-linear behaviour of the materials, but if deformations are small, in most of the cases, it can be approximated with linear model and in this work we make this assumption too. Consequently, we are interested mostly in the first part of the curve and do not analyze non-linearity.

2.2 Model of Kelvin cell

In nature, foam is a porous substance, containing bubbles of gas. Since it has a wide application in different industrial areas, a lot of research was conducted to understand mechanical properties of such materials. In pursue to analyse them, theoretical models of the underlying microcstructure were developed. In the past, they were used to model mechanical properties, but in this work we show how to use one of these microstructures not for analysis, but rather for synthesis. The *tetrakaidecahedron* (or *Kelvin cell* [Thompson, 1887]) is a a polyhedron with 14 faces comprised of six quadrilateral and eight hexagonal faces:

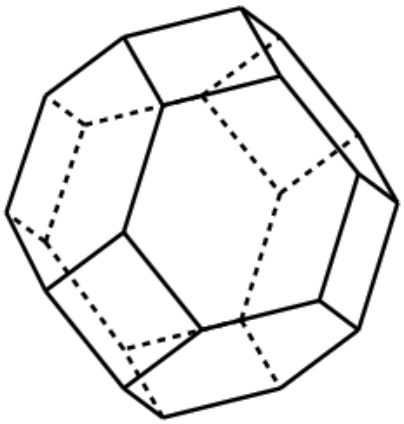

FIGURE 2.2: Tetrakaidecahedron

Advantages of using this model are two-fold. Firstly, it allows for an easy and elegant construction. Foams are the object of study for material scientists. In order to simulate its growth, they use Voronoi Diagram (VD). This is a widely used tool for analysis of open-cell elastic foams[Zhu, Knott, and Mills, 1997]. Formally, it is defined as a partitioning of space into regions, where points of one region are closer to this region than to any other. Interestingly, by imposing a specific pattern on position of seeds, one can achieve different regular microstructure packing of the space. For example, if we imagine the space to be subdivided into a cubic cell grid and place a seed in every corner and center of each cubic cell (Fig. 2.3), the obtained VD will result into tetrakaidecahedron. It allows us to parametrize foam by the side length a of the cubic cell.

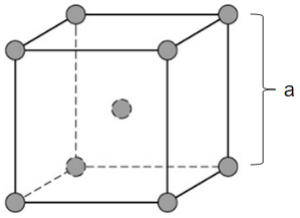

FIGURE 2.3: Body-centered-cubic packing

Another advantage of Kelvin cell is its best isotropy value among other packing patterns [Luxner, Stampfl, and Pettermann, 2007]. However, even higher isotropy can be achieved by foams that have irregular structure. Approach of [Martínez, Dumas, and Lefebvre, 2016] follows this idea, but basing on [Babaee et al., 2012], regular structures lose its durability in terms of yield strength when irregularity is introduced. Thus, favouring regular Kelvin cell we sacrifice isotropy, but achieve higher durability.

2.3 Mechanical models for prediction of elastic properties

To use foams for fabricating objects with desired stiffness, we first need to understand how to control it. Different theoretical models of foam predicting mechanical properties were developed. They use different deformation mechanisms as the defining ones for mechanical behaviour of microstructure. Mostly, they are based on beam theory, assuming axial and bending rigidity of each strut.
In [Gibson and Ashby, 1989] (G&A) a general formula for open-cell foams is given as

$$E = E_s C \gamma^2, \tag{2.4}$$

where E_s stands for stiffness of base material, C is a constant and γ is a relative density. The constant C can vary, depending on the structure's geometry and other factors (e.g. non-uniform cross-sections of struts). One of the models that is more precise in its formulation is given by [Zhu, Knott, and Mills, 1997]:

$$E = \frac{0.60021 \cdot E_s \cdot \gamma^2}{1 + 0.9003 \cdot \gamma} \tag{2.5}$$

Expression (2.5) depends on two parameters: Young's modulus of the base material E_s and the relative density of the foam γ, which is a ratio between the volume of solid material in the foam and the whole volume occupied. Since we know exact geometry of the Kelvin cell, we can give an assessment on relative density of the foam by computing γ for a single cell. [Sullivan, Ghosn, and Lerch, 2008] give the expression that relates γ to the length L of the tetrakaidecahedron's edge:

$$\gamma = \frac{3A}{2\sqrt{2}L^2}, \tag{2.6}$$

where A is a cross-section area. Expression (2.6) also depends on the type of the cross-section of the beam. Here and further, we consider only model with circular cross-section.

It is important that treatment of struts as beams imposes a certain limitation on

the cell geometry. The ratio of length to width should be at least three. This requirement places an upper limit on the relative density of the foam for which the model predictions will be valid. According to the experiments, conducted in [Zhu, Knott, and Mills, 1997], relative density should not exceed 10-15%. Beyond that limit, predictions start to be unreliable.

2.4 Validation of models

In order to validate models, proposed in the previous section, we fabricate several samples representing unit material tiles (Fig. 2.4) and measure their Young's modulus. The details of fabrication process will be given in the next section. Now, we want to describe the setting of performed measurements. Since the construction of Kelvin cell foam is based on the packing of seeds in cubic cell, we will differentiate them by the side length of the unit cell's enclosing cube (Fig. 2.3). Relation between the Kelvin cell's edge length L and the edge length a of enclosing cube is given by

$$L = \frac{a\sqrt{2}}{4}. \tag{2.7}$$

We have printed three cubic samples with different edge length of the enclosing cubic cell: 2.5, 2.65, 2.8 mm. All struts have the same cross-section area - a circle of radius 0.15 mm. This is the minimal printable cross-section we achieved that was also used by [Martínez, Dumas, and Lefebvre, 2016].

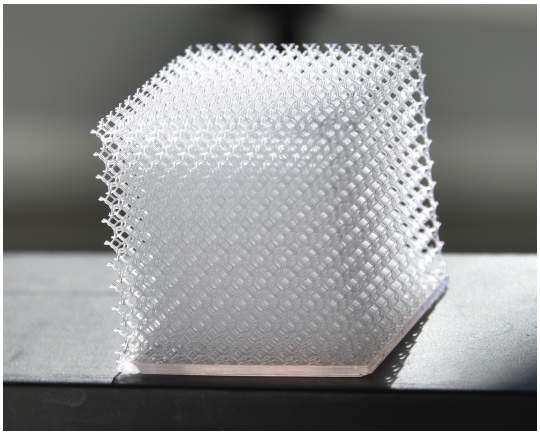

FIGURE 2.4: Kelvin cell foams sample

In order to assess elastic behaviour of the samples we used an uniaxial compression test. For this purpose, we used a machine (Fig. 2.5) that consists of a sensor and a pressing plate, which is actuated by two motors. When the plate presses the object, we know exact displacement of a step, and for every step sensor records the value of force with which the object resists compression. Using this setup, we can record a force-displacement (FD) data, from which we obtain a stress-strain curve. By fitting the curve to a line and taking the inclination coefficient, we can extract Young's modulus E.

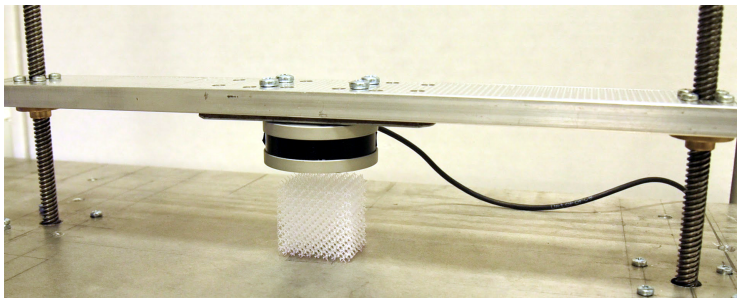

FIGURE 2.5: Uniaxial Test Machine

Knowing Young's moduli of our samples set, we tried to validate several models (Fig. 2.6). Apart from the material science models described in previous section, we also tried to fit other function in order to catch dependance between cell size and its Young's moduli for further use.

The model of Zhu (2.5) stongly disagreed with our data. Though being specifically developed for Kelvin cell, the validation provided in [Zhu, Knott, and Mills, 1997] is performed not by comparison with measurement of actual foams, but from simulations, which pushes this model farther from actual context. In contrast, the general model of Gibson & Ashby (2.4) for cellular structures yielded a good fit, since it had a free parameter that allowed us to fit model according to the data.

The best fit was obtained by the 3rd degree polynomial. Apart from passing through the whole sample set, this choice is also important, because unlike the other functions that we tried (higher degree polynomial, exponential function) it is monotonous and passes through coordinate system origin, which obeys a physical sense.

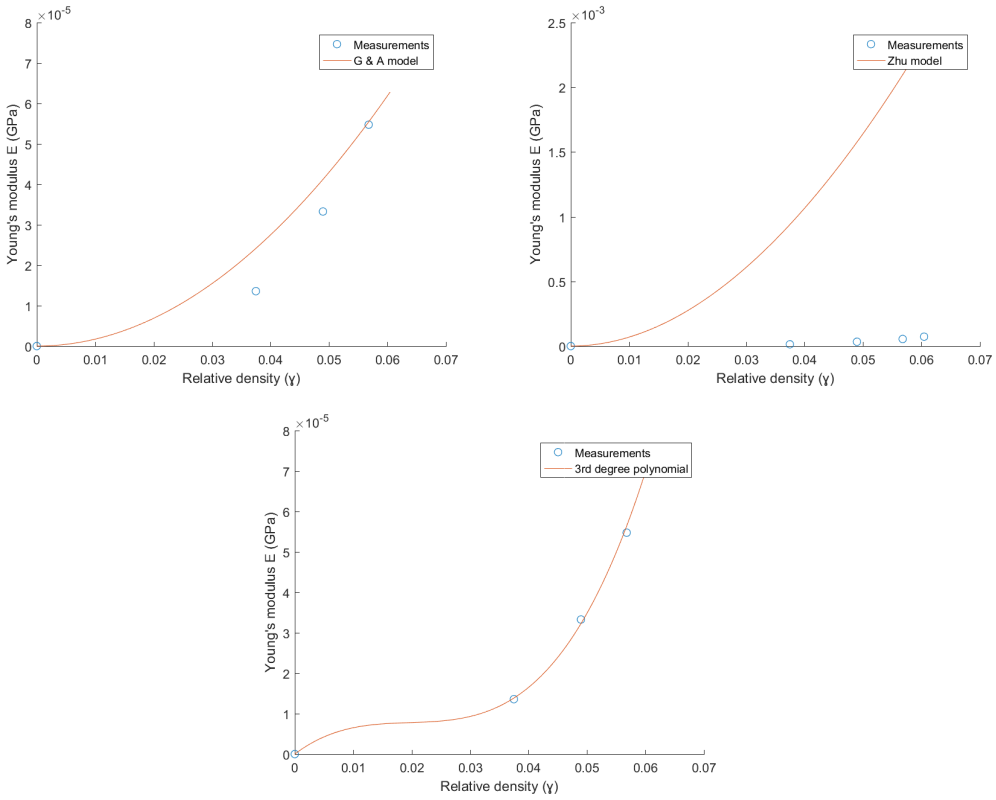

FIGURE 2.6: Model fitting

Behaviour of the Zhu and G & A models can be explained by several reasons. First, technology that we used for printing imposes certain constraints that do not allow the size of printed cubes to be more than 3.5 cm. The Kelvin cells, in their turn, do not scale and should have a fixed size to possess desired properties. Since the cube sample has to be tiled fine enough to exert average elastic behaviour, we are limited in the range of Kelvin cell sizes we can achieve. As a consequence, the length-width ratio in the samples that we fabricated was between 3 and 4. Taking into account restriction mentioned in Section 2.2, it means that we were operating on the edge of reliable predictions. It is also bolstered by the fact that in more finer samples we could observe rapid increase in stiffness.

Next factor that could affect elastic behaviour are the artifacts of fabrication process. Under the microscopic study, they look like a stack of small plates (Fig. 2.7). The structure of such beams can behave differently from the classic beams.

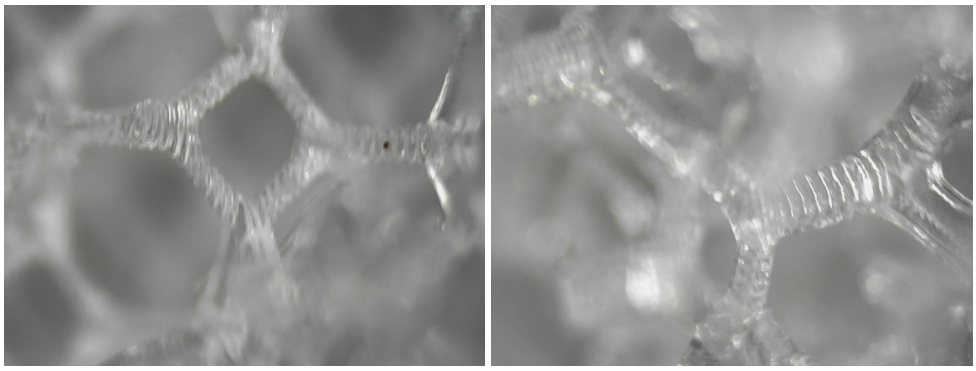

FIGURE 2.7: Photos of fabricated foam in 40x zoom

2.5 Fabrication of the foam

Technology that we use for fabrication is DLP printing, which belongs to the class of additive manufacturing. In this approach, object is printed layer by layer by solidifying resin undergoing UV light radiation. Thus, we need to supply a stack of images that represent slices of the object. In this chapter we want to describe, how we render these images.

Usually, one uses existing software to generates slices. However, output of the Voronoi Diagram generation is a collection of line segments, which can be assigned to an arbitrary thickness. Existing software performs slicing by cutting every triangle of the mesh with a plane. If we convert these segments to solid cylinders, then some artifacts can arise, e.g. cutting plane can go through a vertex or edge of a triangle. Also, processing of such a fine mesh would take a significant amount of time.

Due to specificity of the geometry of objects that we print, we implemented a slicer that takes it into account. Slices represent images of a fixed resolution. We query each pixel of each slice and check, whether any line segment intersects the point. If yes, we color pixel with white. Otherwise, we leave it black. Checking intersection is done by a simple geometrical test.

In order to accelerate rendering, we employ two improvements. When we process a slice, we consider only those segments that are intersected by the plane formed by the slice. We presort segments according to Z coordinate, having second point of segment be always non-lower than the first one. Next, in order to not traverse the

whole canvas, we compute a bounding box for each line segment, intersecting current plane, and go only within this box. We take left-upper- and right-bottom-most values of segment endpoints coordinates and perform line-plane intersection check only within the rectangular region.

Algorithm 1 Slicing

Input : edges of Voronoi Diagram
Output : stack of images

$\tau \leftarrow$ *radius of the beams cross-section*
sortSegments()
for k = 1..n **do**
    $segments \leftarrow initializeSegments(k)$
    for idx = 0... | segments | **do**
        $s = (a, b) \leftarrow segments[idx]$
        $s\_norm \leftarrow ||s||$
        s.normalize()
        $leftMargin \leftarrow min(a.x, b.x)$
        $rightMargin \leftarrow max(a.x, b.x)$
        $topMargin \leftarrow min(a.y, b.y)$
        $bottomMargin \leftarrow max(a.y, b.y)$
        for q = ($leftMargin, topMargin$)..($rightMargin, bottomMargin$) **do**
            $t \leftarrow (q_p - s.a) \cdot s$
            if $t < -\frac{\tau}{2}$ **or** $t > \frac{\tau}{2} + s\_norm$ **then**
                continue
            end if
            $q_p \leftarrow s.a + t \cdot s$
            if $||q_p - q|| \leq \tau$ **then**
                make the pixel (i,j) white
                break
            end if
        end for
    end for
end for

Chapter 3

Heterogenous foam

In previous chapter we described the pipeline of fabrication of homogenous foams. Now, we want to move to more challenging case - generation of foams with spatially-varying deformation behaviour. First, we describe how to generate such a foam given a map of Young's moduli. Then, we give a description of method proposed by [Xu et al., 2015] to derive the Young's moduli map from the user-specified load-deformation behaviour.

3.1 Elasticity control

Researchers approached the problems of spatial-varying elastic properties in different ways. [Panetta et al., 2015] used to generate families of microstructures by specific parametrization of nodes and struts, which allowed to average neighboring cells to connect them. [Schumacher et al., 2015] used to populate space of possible microstructures by continuously interpolating structures that are close to each other in terms of elastic properties. Having several different candidates for a single material property allowed to formulate connectivity problem as an assignment problem, minimizing discrepancies between neighboring cells. In [Martínez, Dumas, and Lefebvre, 2016], authors did not have explicit connectivity problem, because resulting foam is being constructed through Voronoi Diagram (VD). They achieve spatially-varying stiffness through placing seeds in an adaptive grid, where subdivision is performed when more seeds should be placed in the region of interest, since denser seeding will lead to a stiffer foam.

Our approach also relies on VD, but in contrast to [Martínez, Dumas, and Lefebvre, 2016] that generates a random foam, we want to achieve a regular structure. Using an adaptive grid would lead to inconsistencies on the boundaries violating the seed packing pattern of Kelvin cell (Figures 4.6 and 4.7). In order to preserve the pattern and also achieve spatial variation of properties, we extend our approach by a specific seeds position computation that will be described in the following section.

3.2 Grid deformation

With use of models that relate stiffness and the size of cube enclosing Kelvin cell (Section 2.2) we can transform the problem of achieveing desired stiffness distirubtion within the target object into geometric context. Our goal becomes to find such a grid that after placing the seeds in it according to the pattern, resulting Kelvin cells will match desired distribution as close as possible.

Posing this task as an optimization problem we have to define the following constituents: domain, objective function and constraints. Since we want to deform a grid, domain is defined as a set P of corner points that comprise it.

The objective function should penalize discrepancies between current cell sizes and the target ones. So, it would be natural to choose a sum of length differences between current cell edge lengths of each cube and the target ones. Concerning constraints, we should take into consideration the shape of cell, since we want it to stay cubic. One way to do it would be to penalize angles between edges that meet at the corner for deviation from $90°$. However, it can cause undesired behaviour in form of disorientation of the grid as a whole relative to the main axes, since cube angles can be correct, even if the whole cube is tilted arbitrarily. To avoid this problem, we modify an objective function to penalize differences between vectors on the edges of target and current cells instead of their lengths. Imagine one grid cube, where there is a vector assigned to each edge (Fig. 3.1). Target cells are always oriented parallel to the main axes and the vectors assigned are just unit base vectors scaled by the target cell size.

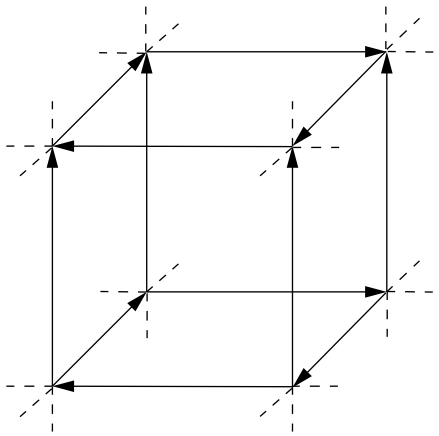

FIGURE 3.1: Grid cell c

Thus, even if the current cubic cell matches the desired size, but is disoriented or inclined, it will be reflected in the value of objective function:

$$\min_{P \in V^o} \quad \frac{1}{2} \sum_{c \in C(P)} \sum_{i=1}^{12} ||\boldsymbol{l}_{i,c} - \boldsymbol{g}_{i,c}||^2, \tag{3.1}$$

where V^o is an interior of the target object, C is a set of cubical cells falling in the interior V^o by at least one of the comprising corner points P, $\boldsymbol{l}_{i,c}$ is one of the 12 vectors lying on of the edges of a cubical cell c in the current grid and $\boldsymbol{g}_{i,c}$ is a corresponding vector on the edge of the cubic cell in the target grid.

The set of target cell sizes is constructed by evaluating model inverse to one of the presented in previous chapter (distribution of the Young's moduli map in section 3.3). The obtained set contains target cell size value for every mesh element. Due to the fact that typically a mesh element is smaller than the target size of cell and the fact that due to cell changing process cells are getting displaced, on every iteration we check for each cell, what is the closest mesh element to the cell centroid and the closest candidate's value will be assigned as a target the size for the cell.

In order to solve optimization problem (3.1) we use *Conjugate Gradient Method* implemented in Poblano toolbox [Dunlavy, Kolda, and Acar, 2010]. We feed the gradient

$$\sum_{c \in C(P)} \sum_{i=1}^{12} (\boldsymbol{l}_{i,c} - \boldsymbol{g}_{i,c}), \tag{3.2}$$

and the objective function to the solver and obtain positions of cells' corner points.

Some results of the grid deformation procedure can be seen on the Fig. 3.2.

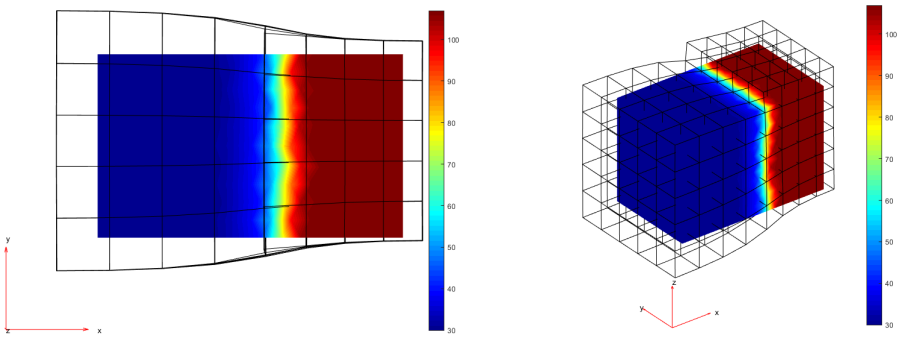

(A) Bottom view (B) Side view

FIGURE 3.2: Grid deformation for simple cuboid

Colors on the cuboid reflect its stiffness. The red part corresponds to the stiffer region, which implies smaller size of cells. On the opposite, in the softer region, colored with blue, cells should possess a bigger size.

Having the deformed grid cells, we can populate them with seeds according to the Kelvin cell pattern (Fig. 2.3), i.e. one seed in every corner and center of each cell, and perform Voronoi Tesselation [Lévy and Liu, 2010], (Fig. 3.3).

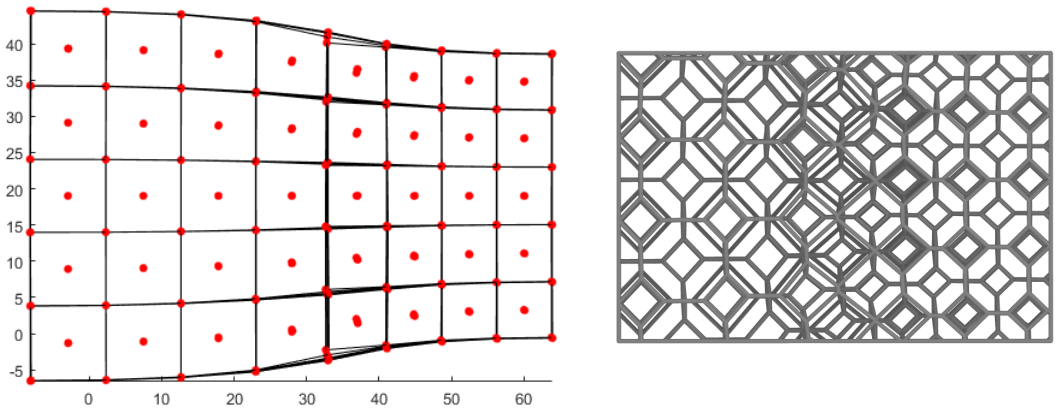

(A) Grid populated with seeds (B) Clipped Voronoi Diagram

FIGURE 3.3: Deformed grid and VD

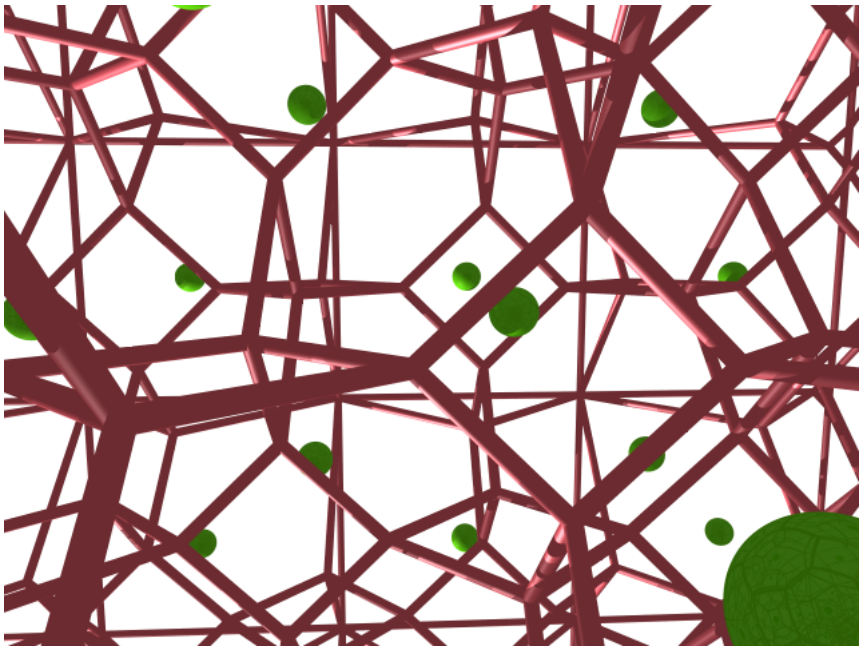

FIGURE 3.4: Render of a Kelvin foam

3.3 Derivation of Young's moduli distribution

In this section we describe the process of obtaining distribution of stiffnesses over the object mesh. In order to achieve a smooth heterogenous distribution, we implemented a technique by [Xu et al., 2015]. In this method, user specifies load-displacement pairs at particular points (Fig. 4.8) and as a result, the algorithm assigns stiffnesses to every element of mesh, such that requirements at points of interest are satisfied and resulting distribution is smooth.

The core of the method lies in solving optimization problem, where Young's moduli are updated in such a way that discrepancies between the loads resulted from simulation based on current Young's moduli and the target loads are minimized.

As an input the user specifies force-displacement pairs in form of "grips", assigning two points on the parts of the object as if it was pinched. The vector connecting these points defines direction of the load. After specifying grips, user assigns magnitude of the applied force along the direction.

We should mention that in the original paper, authors perform optimization in two steps: one is actual *material optimization* for satisfying force-displacement constraint and the second one is *handle position optimization*, which updates a position of the handles. Since we assume that load points stay the same throughout the whole process, we do not consider this second phase and focus only on material optimization problem.

3.3.1 Simulation

The simulation process is one of the key components of the employeed method. In general, problem of analysing how a certian object will be deformed under a certain load is called an elastostatic problem and is formulated as the following boundary-value problem (BVP):

$$-\nabla \cdot \sigma = f, \qquad \text{in } \Omega \tag{3.3}$$

$$\sigma = C : \frac{1}{2}(\nabla u + \nabla u^T), \qquad \text{in } \Omega \tag{3.4}$$

$$u = 0, \qquad \text{in } \Gamma_D \tag{3.5}$$

$$\sigma \cdot n = g_N, \qquad \text{in } \Gamma_N \tag{3.6}$$

where σ is an internal stress resisting external load f in the body Ω, f is a load vector, C is an elasticity tensor, which basically encodes information about elastic properties, u is a displacement vector and n is a normal along the object's contour. Equations (3.5) and (3.6) stand for boundary conditions, where the boundary is split on two segments Γ_D and Γ_N. On the first segment, the so-called Dirichlet conditions are defined, which fix the exact displacement in the region. The latter segment, Γ_N, corresponds to Neumann conditions that require loads to take values of g_N along the normal n.

A common approach to solve this BVP numerically is a Finite Element Method (FEM): one projects function of u on the space of piece-wise linear functions, splitting problem domain on "finite elements" (tetrahedrons, in our case). This method allows us to reformulate original problem (3.3-3.6) as a sparse linear system that one can efficiently solve. We use a common notation for the linear system: K is a stiffness matrix, f is a load vector and u is a displacement vector. Thus, FEM problem is

stated as

$$Ku = f \tag{3.7}$$

By construction, the stiffness matrix K depends on two main elasticity parameters: Young's moduli E and Poisson's ratio ν. So, correct functional notation for K should be $K(E, \nu)$, but since ν is assumed to be constant and dependance on E can be understood from context, in some places they are omitted and for simplicity we will use K instead of $K(E, \nu)$.

The boundary conditions (3.5-3.6) are considered in the linear system (3.7) in the following way: Dirichlet conditions are realized through a large penalization term - by adding a large value to entries of K that correspond to the fixed elements. Second type of boundary conditions - Neumann conditions are realized through an actual assignment of load values at the corresponding entries of the load vector f.

3.3.2 Static condensation

Since user assigns displacement-load pairs only on a particular parts of object, from the FEM point of view, we are not interested in what will happen on elements, where no loads are assigned. Hence, we would like to reorder lines of the linear system to get a direct relationship between current displacement and loads at target elements. A procedure for it is commonly referred as a *static condensation* [Guyan, 1965].

We split load vector f in two parts: $\bar{f}$ - loads specified by user and $\hat{f}$ - free loads, that can be assumed to be zero or any other force. Same logic is followed in convention on displacements $\bar{u}$ and $\hat{u}$. Thus, the linear system $K(E)u = f$ can be rewritten as:

$$\begin{bmatrix} K_{11}(E) & K_{12}(E) \\ K_{21}(E) & K_{22}(E) \end{bmatrix} \begin{bmatrix} \hat{u} \\ \bar{u} \end{bmatrix} = \begin{bmatrix} \hat{f} \\ \bar{f} \end{bmatrix} \tag{3.8}$$

Then, using block-Gaussian elimination, one can express relation between displacement $\bar{u}$ and loads $\bar{f}$ on constrained vertices following steps:

$$\begin{aligned} K_{11}(E) \cdot \hat{u} + K_{12}(E) \cdot \bar{u} &= \hat{f} \\ K_{21}(E) \cdot \hat{u} + K_{22}(E) \cdot \bar{u} &= \bar{f}, \end{aligned} \tag{3.9}$$

$$\begin{aligned} K_{11}(E) \cdot \hat{u} &= \hat{f} - K_{12}(E) \cdot \bar{u} \\ \hat{u} &= K_{11}^{-1}(E) \cdot (\bar{f} - K_{12}(E) \cdot \bar{u}) \end{aligned} \tag{3.10}$$

Substituting $\hat{u}$, we arrive at

$$K_{21}(E) \cdot K_{11}^{-1}(E) \cdot (\hat{f} - K_{12} \cdot \bar{u}) + K_{22} \cdot \bar{u} = \bar{f} \tag{3.11}$$

$$K_{21} \cdot K_{11}^{-1} \cdot \hat{f} - (K_{21} \cdot K_{11}^{-1} \cdot K_{12} - K_{22}) \cdot \bar{u} = \bar{f} \tag{3.12}$$

$$(K_{22} - K_{21} \cdot K_{11}^{-1} \cdot K_{12}) \cdot \bar{u} = \bar{f} - K_{21} \cdot K_{11}^{-1} \cdot \hat{f} \tag{3.13}$$

Taking the term in front of $\bar{u}$ as $\bar{K}$, we rewrite last equation as

$$\bar{K} \cdot \bar{u} = \bar{f} - K_{21} \cdot K_{11}^{-1} \cdot \hat{f} \tag{3.14}$$

Thus, we arrive at a linear system that encodes relationship between displacements and loads on constrained vertices only. Since our goal is to know what forces

are exerted under given deformation, we arrive at the expression for the $\bar{f}$ as

$$\bar{f} = \bar{K} \cdot \bar{u} + K_{21} \cdot K_{11}^{-1} \cdot \hat{f} \tag{3.15}$$

3.3.3 Optimization Problem

Following [Xu et al., 2015], our goal is to obtain such a distribution of Young's moduli **E** that it will match desired constraints and will be smooth. Authors present an objective function that satisfies these requirements:

$$\min_{E} \quad \frac{1}{2} E^T L E + \frac{\alpha}{2} ||\tilde{f}(E) - \bar{f}||^2, \tag{3.16}$$

$$\text{where} \quad \tilde{f}(E) = \tilde{K}(E) \cdot \tilde{u} + K_{21}(E) \cdot K_{11}^{-1}(E) \cdot \hat{f} \tag{3.17}$$

Optimization problem (3.16-3.17) penalizes discrepancy between the current vector of load $\tilde{f}$ and a specified $\bar{f}$. We want to notice that the expression (3.17) is an equivalent version of the expression (3.15) with only difference that instead of relating fixed forces and displacements, it relates its values on the current iteration.

Apart from the main term, objective function (3.16) contains a smoothness energy term, which is defined as a an energy of a discrete mesh Laplacian. Authors discuss different variations (e.g. weighted mesh Laplacian). Since they do not observe much difference, they use a standard discrete mesh Laplacian:

$$(LE)_i = \sum_{j=1}^{m} \omega_{i,j}(E_i - E_j), \tag{3.18}$$

where m is a number of tetrahedrons and $\omega_{i,j}$ is 1 if tetrahedrons i and j share a vertex, and 0 otherwise.
Constant α in (3.16) regulates importance of the force matching term. Since smoothness energy term can often be overweighting, in order to enforce importance of constraint satisfaction, we set it to a value around 10.
We approach the optimization problem (3.16) with conjugate gradient method, using implementation from Poblano toolbox [Dunlavy, Kolda, and Acar, 2010]. Additionally to the objective function, a gradient is provided, which is defined as

$$LE + \alpha(\frac{d\hat{f}(E)}{dE})^T \cdot (\hat{f} - \bar{f})), \tag{3.19}$$

$$\text{where} \quad \frac{d\tilde{f}(E)}{dE_e} = \begin{bmatrix} K_{21}(E)K_{11}^{-1}(E) & -I \end{bmatrix} \frac{dK}{dE_e} \begin{bmatrix} K_{11}^{-1}(E)(K_{12}(E) \cdot \bar{u} - \hat{f}) \\ -\bar{u} \end{bmatrix}, \tag{3.20}$$

for every $e = 1, ..., m$, i.e. for every element.

Term $\frac{dK}{dE_e}$ is a derivative of stiffness matrix K over individual Young's modulus of element e, on which K depends linearly. It can be obtained by computing K having Young's modulus of element e set to 1 and zeroing all the other elements.

3.3.4 Model reduction

Original problem (3.16) is a high-dimensional one. It optimizes for vector E of length equal to number of finite elements in the mesh, which can be up to several thousand for a reliable simulation. One of the contributions made by the [Xu et al., 2015]

is to optimize not for a vector of Young's moduli E, but instead using so-called *material vectors*. These are obtained through decomposition of E on a subspace of eigenvectors of mesh Laplacian:

$$E = \Phi z, \tag{3.21}$$

where Φ is a matrix of first r eigenvectors, obtained by solving generalized eigenvalue problem:

$$Ly_i = \mu_j V y_j, \tag{3.22}$$

where y_j is an j-th eigenvector, μ_j is a corresponding eigenvalue and V is a per-element volume matrix.

Applying (3.21) to the (3.16), optimization problem becomes

$$\min_z \quad \frac{1}{2} z^T Q z + \frac{\alpha}{2} ||\tilde{f}(z) - \bar{f}||^2, \tag{3.23}$$

$$\text{where} \quad \tilde{f}(z) = \tilde{K}(z) \cdot \bar{u} + K_{21}(z) \cdot K_{11}^{-1}(z) \cdot \hat{f}, \tag{3.24}$$

$$Q = \Phi^T L \Phi \tag{3.25}$$

The gradient of the objective function turns into

$$Qz + \alpha(\frac{d\tilde{f}(z)}{dz})(\tilde{f}(z) - \bar{f}), \tag{3.26}$$

$$\text{where} \quad \frac{d\tilde{f}(z)}{dz} = \sum_{e=1}^{m} \frac{d\tilde{f}(z)}{dE_e} \Phi^e = HG\Phi, \tag{3.27}$$

$$\text{taking} \quad H = \left[K_{21} K_{21}^{-1} - I\right] \tag{3.28}$$

and G consisting of columns

$$\frac{d\tilde{K}}{dE_e} \begin{bmatrix} K_{11}^{-1}(K_{12}\bar{u} - \hat{f}) \\ -\bar{u}. \end{bmatrix} \tag{3.29}$$

Chapter 4

Results

In this chapter, we want to present results of the experiments concerning the claims that we made in this thesis. The main claim is that Kelvin structure yields more durable and sustainable behaviour than the analogous structures - Random Voronoi Foam (RVF) from [Martínez, Dumas, and Lefebvre, 2016]. We evaluate durability by both simulating structures and fabricating representative samples. In the first section we describe results of physical simulations of the deformation of two kinds of foams : Kelvin foam and RVF. In the next section, we present durability tests on the actual printed samples. We make measurements of their stiffness and see how it changes after repeated tests. Second part is devoted to the behaviour of heterogenous foams. We analyze effects of grid deformation and compare the cases where two regions of different stiffnesses transit. Finally, we show the results of Young's moduli distribution optimization on the sample mesh.

4.1 Stress distribution simulation

For the simulation we took two samples that have similar stiffness : Kelvin cube with the unit cell size 2.8 mm and strut thickness 0.25 mm and RVF cube with relative density 33 and strut thickness 0.3 mm. We modeled them as beam connected structure in the ABAQUS simulation package. As boundary conditions, we set their bottom to be fixed and top to be displaced by 1 mm down. The results of the simulation you can see in the Fig. 4.1.

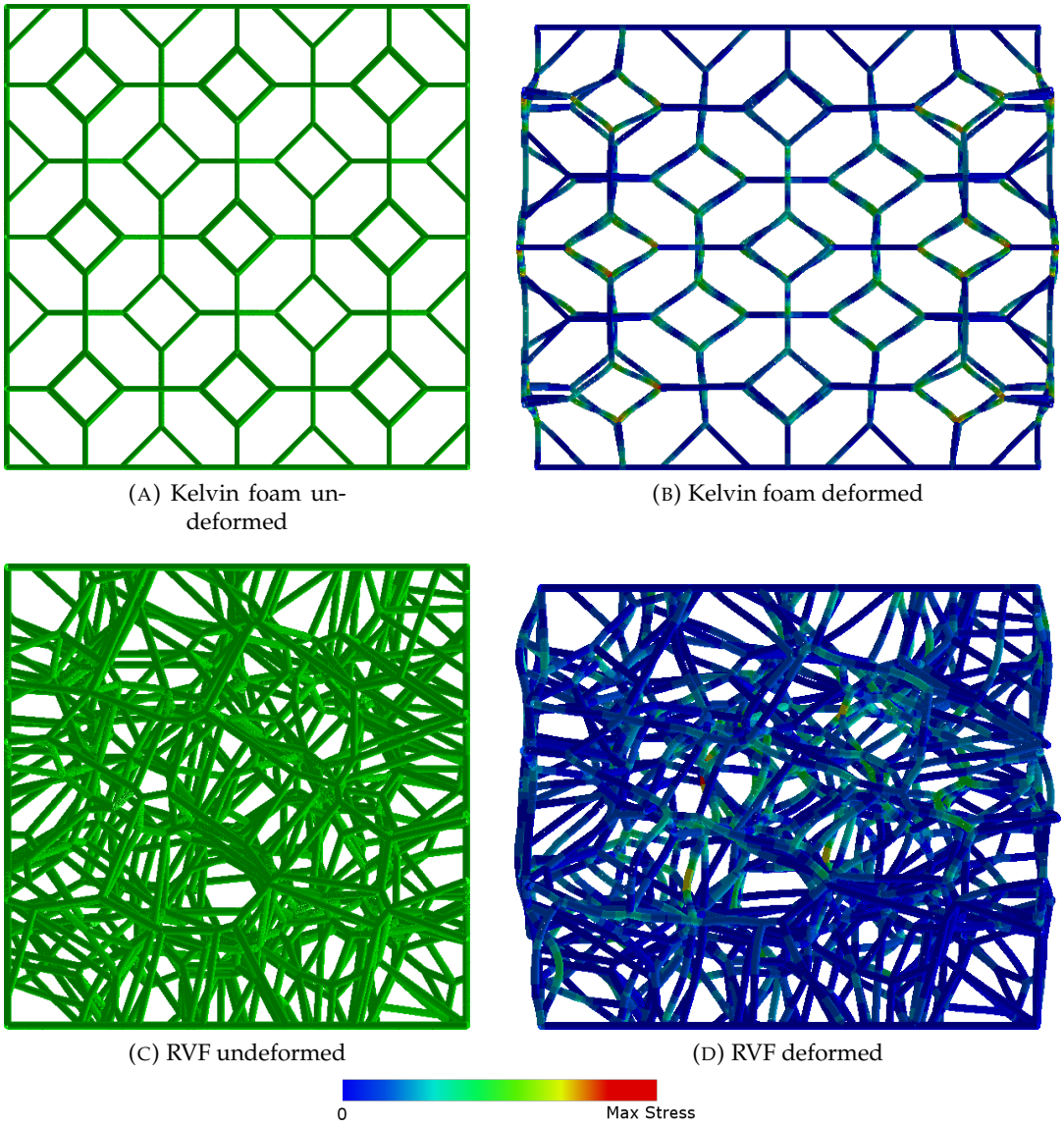

(A) Kelvin foam undeformed

(B) Kelvin foam deformed

(C) RVF undeformed

(D) RVF deformed

FIGURE 4.1: Simulations of compression of foam samples

Visualizations of the deformed cubes are both scaled to the range between zero and maximal stress. In the center of RVF sample you can see one red and few yellow regions, which mean that stress in this structure is very localized. "Red" beams carry the main load, while many others beams are almost inactive. In contrast, for Kelvin cells, load is concentrated mainly in the nodes and is distributed among neighboring cells, which is additionally illustrated by the distribution of loads within simulated structures (Fig. 4.2). Probabilities to meet lower load values for Kelvin foam are concentrated from 0 to 3N, whereas RVF possesses bigger probabilities for higher stress values.

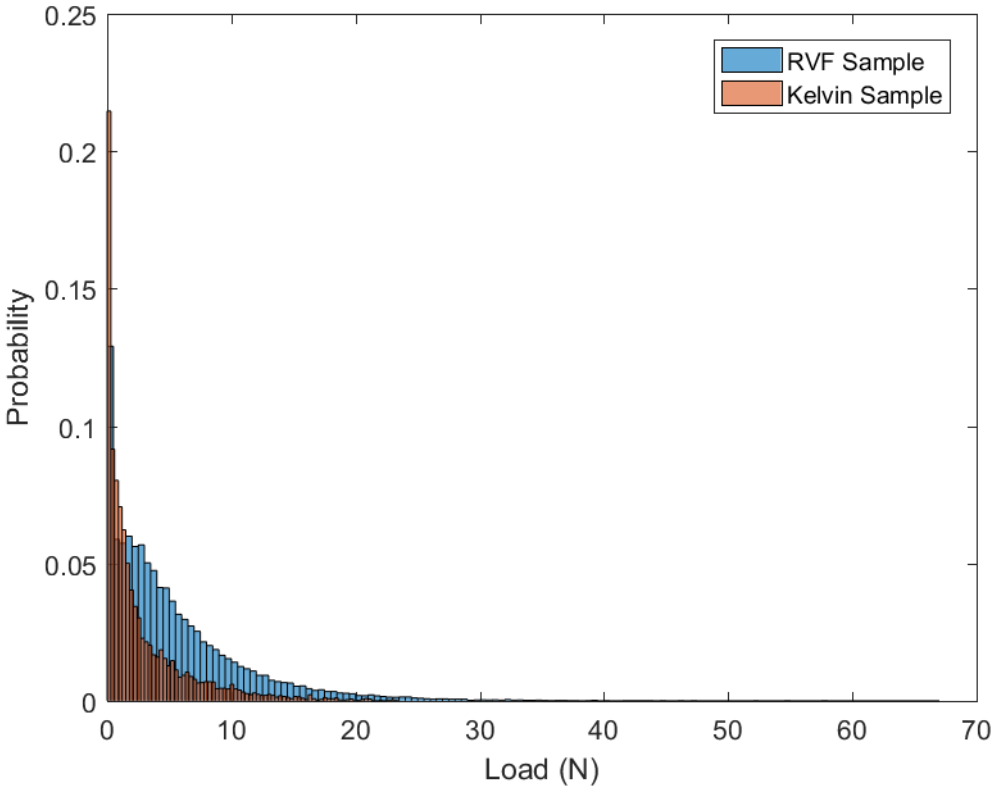

FIGURE 4.2: Histograms of loads within the deformed samples from the Fig. 4.1

4.2 Durability tests

One way to assess durability of the object would be to construct its sress-strain curve and look for a breakage point on the plot, which corresponds to a decrease in resisting force (point C in the Fig. 4.3).

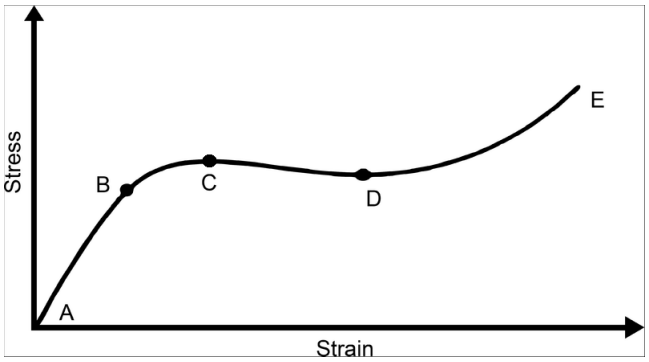

FIGURE 4.3: Stress-Strain curve

However, the breakage point is not always explicit on the plot, as it was in our case. To show a rapid decrease in resistance, object should change its form to high extent. Our objects are truss structures, consisting of thin beams that can break eventually, one by one, rather than together at once. Therefore, decrease in force is rather a series small breaks, which are hard to detect on the plot.

Due to the reasons stated above, we test the structures durability by repeated uniaxial compression tests (Section 2.4) with increasing displacement magnitude. We start with one millimeter, then increase it on every next trial by one millimeter more: two, three and so on, till we compress the object up to half of its height. This approach is motivated by the fact that if the object broke a bit during the test, then in the next measurement it will be a bit softer. Looking at how many of stress-strain curves look similar to each other and at which point we can observe a significant decrease in stiffness will allow us to judge the ability of the structure to resist stress, therefore, its durability.

We prepared two samples, one representing Kelvin structure and one representing Random Voronoi Foam (RVF). For the tests, two samples should have similar stiffness values. We took Kelvin cube with even higher stiffness compared to RVF, since for a stiffer cube there is a higher risk to get broken during equivalent deformations.

First series of compression tests were performed on the RVF (Fig. 4.4). You can observe 10 stress-strain plots. Each curve corresponds to the test with particular strain, increasing from 3% to 35%. Normally, to assess the linear behaviour of the object, it is a common practice to take up to 5% strain to evaluate its Young's moduli [Bickel et al., 2010]. Therefore, we mainly focus our attention on this region. The plots #1-5 are similar and have close inclination coefficient. However, you can see that already after the first trial there is a reduction in stiffness. Every next plot does not collide with the previous one, which means that the object gets softer after every test. Finally, on the test #6, the more significant stiffness fall can be observed, which means that the object underwent plastic deformation after going through 20% strain during the test #5.

As was discussed in the previous section, sequential decrease in stiffness can be explained by the localized stresses, concentrated on the few struts, that carry the main load. After one of such struts break, load concentrates on the next one, but the overall structure loses its initial stiffness and becomes softer.

One can notice that plots in Fig. 4.4 contain negative Young's moduli at the starts of stress-strain curves. This behaviour is due to the measurement device. If, after the uniaxial test, sample undergoes plastic deformation, i.e. gets broken, it does not completely restore its original state. The object does not touch the force sensor anymore, which being set with the certain value in the beginning of experiments will show negative force values.

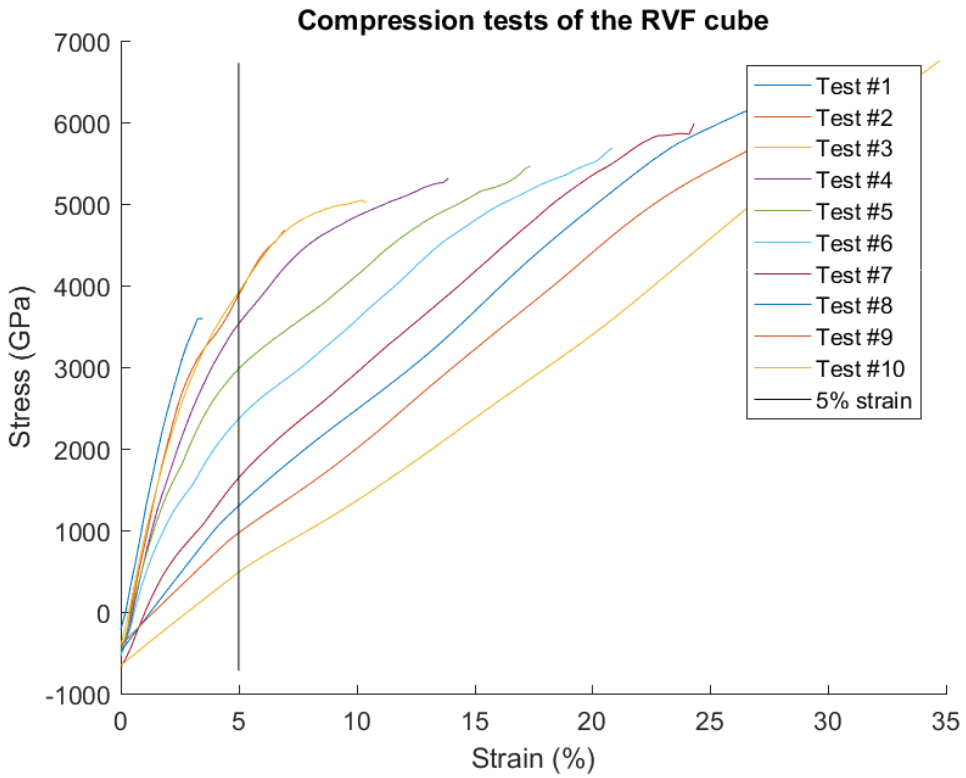

FIGURE 4.4: 10 sequential uniaxial compression tests on the RVF cube with the density of 37 seeds per cube

The Fig.4.5 depicts stress-strain curves for the compression tests on the Kelvin cube. You can see that curves from 1 to 7 are very similar even beyond 5% strain. First change occurs only during the test #8, but before 5% it is still similar to previous tests. On the tests #9-10 we can see the first significant decrease in stiffness. Loading the sample by compressing it beyond 27% causes crushing. It can be seen on the following tests #9-10, where the curves' incline reduces drastically.

From the presented results, we can conclude that the Kelvin foams exhibits higher durability than the Random Voronoi Foams (RVF). It was demonstrated that the Kelvin foam had a higher rate of stiffness preservation after the compression tests, whereas RVF started to break after first interactions.

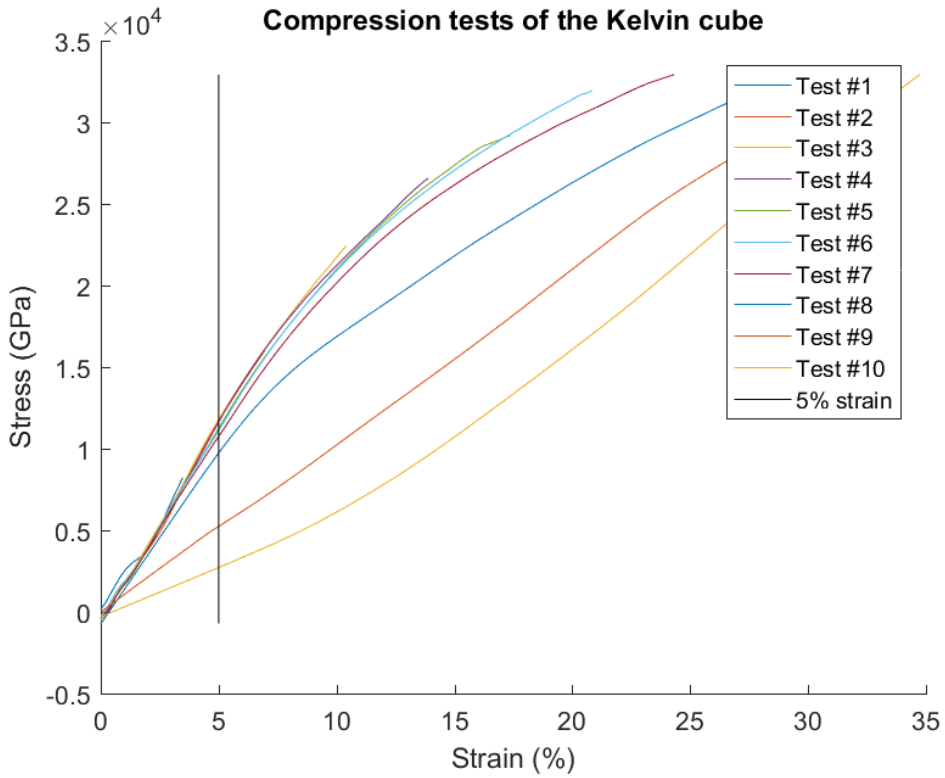

FIGURE 4.5: 10 sequential uniaxial compression tests on the Kelvin cube with cell size 60 pxls

4.3 Transitions in heterogenous foam

To analyze the technique proposed in Section 3.2, we compare one case generated by two different approaches. The case is a heterogenous foam sample consisting of two regions that meet in the middle. The left region is supposed to have cell sizes 9 mm and the right region - 6.5 mm, i.e. on 30% smaller.

Two techniques for generating heterogenous foam differ in the approach of placing seeds. In the first one, described in Section 3.2, seeds are placed so that cubical cells transit smoothly between regions. In the second approach, we place them keeping the pattern and cell sizes only within target regions. To compare two techniques we present renders that illustrate both techniques in the Fig. 4.6.

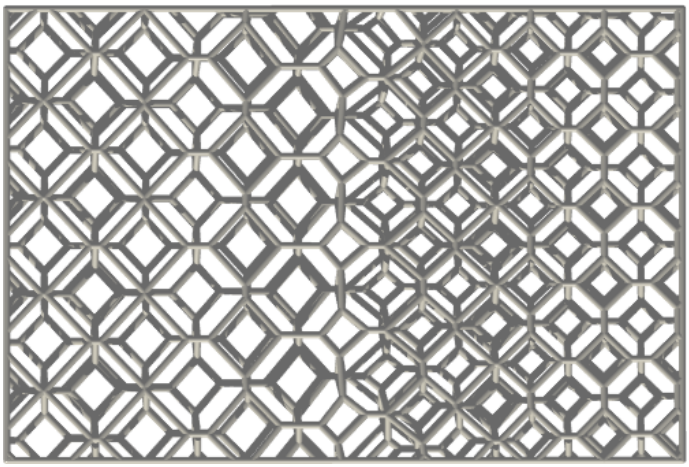

(A) Smooth transition

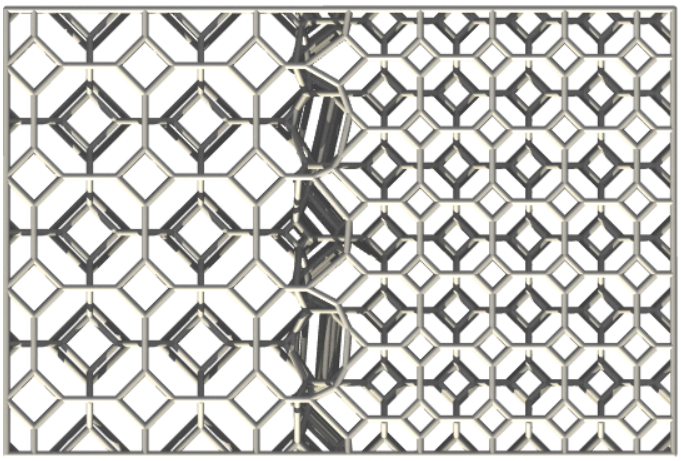

(B) Hard transition

FIGURE 4.6: VD-generated cuboid foams with different transitions

You can see that in case of hard transition cell sizes are much more accurate than in smooth transition case. However, it possesses two major issues. First, transition region has a lot of excessive edges (Fig.4.7) that causes additional stiffening. Second reason is that, usually, the description of desired elastic properties within the object is given as a smooth map, which after discretization can give a rise to several sequential transition regions that will be surrounded by the walls of additional struts. Using our approach allows to adapt the structure to a given map of cell sizes continuously with minimal distortions.

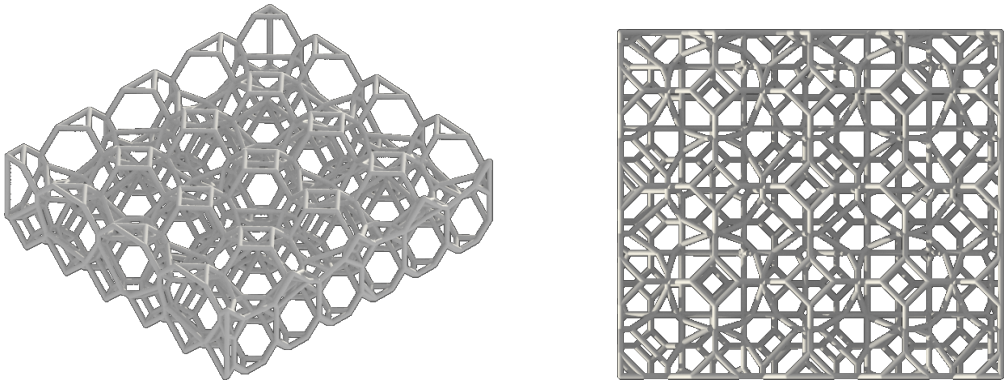

(A) Side view (B) Top view

FIGURE 4.7: Cut of the transition part from the Fig. 4.6b

4.4 Optimization of Young's moduli distribution for deformation behaviour

Generating map of Young's moduli from the user-specified deformation behaviour is an important part of the pipeline. To demonstrate approach of Xu et al., 2015 we used a model of a teddy bear as an example. We selected nodes of the mesh and assigned different loads to them, imposing unit displacement (Fig. 4.8). For the paws, we assigned the loads equal to 5N, for the head 4N and for the belly 2N. That is, we wanted to achieve stiffness map that corresponds to hard head and paws and a soft belly.

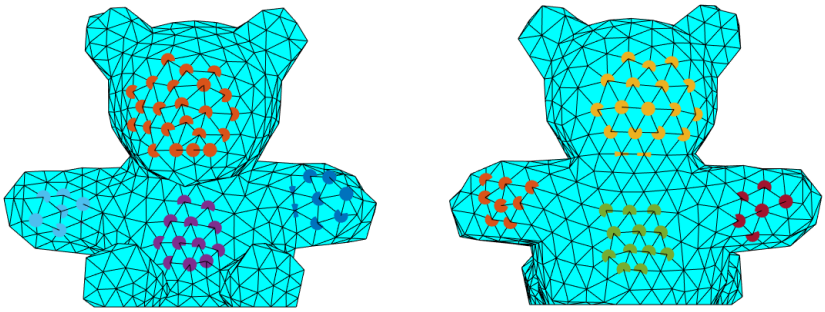

(A) Front view (B) Back view

FIGURE 4.8: Selected nodes

In the Fig.4.9 you can see visualization of Young's moduli map as a color map. As expected, parts of the object got desired stiffness values.

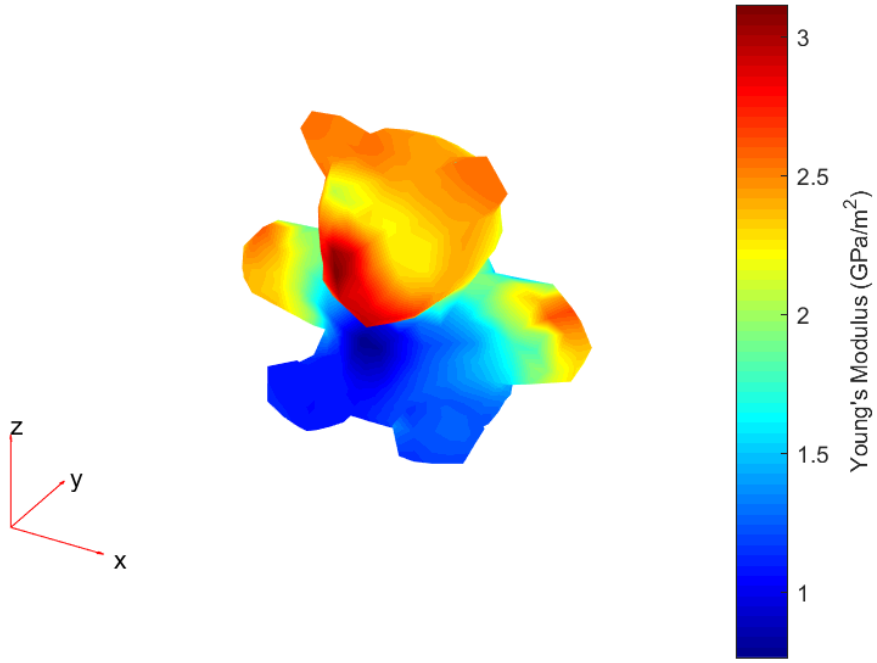

FIGURE 4.9: Young's moduli distribution

Additional information can be seen in the Fig. 4.11. It depicts the target loads and the obtained forces for the mesh nodes for which user specified the behaviour. Two force sets match each other with acceptable degree of precision.

Having the Young's moduli map, we performed further steps of the pipeline: grid deformation, population with seeds, generation of Voronoi Diagram, slicing and 3D printing. Final result you can see in the Fig. 4.10.

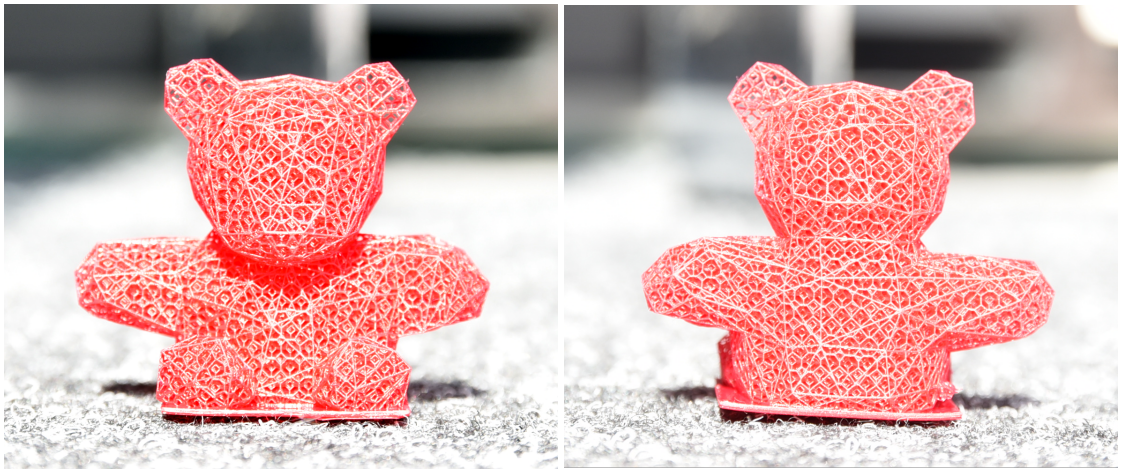

(A) Front view (B) Back view

FIGURE 4.10: Fabricated teddy bear

FIGURE 4.11: Target forces and resulting forces

Chapter 5

Conclusion

In this thesis we presented a new approach to generate foam cellular structure using Kelvin cells. We claimed that it posesses higher durability than analogous solutions and demonstrated it through a series of experiments.

From the physical simulations we analyzed how intrinsic forces are distributed within the structure. It had shown that the problem of localized stresses in Random Voronoi Foam, proposed in [Martínez, Dumas, and Lefebvre, 2016], is not presented to the same extent in our foams. The Kelvin foam exhibits more even distribution of the loads.

In order to assess durability of the structure we made a series of tests. In these experiments we were conducting repeated uniaxial compression test. After each test, we were increasing depth of compression. Presented results show that Kelvin structure is more durable than RVF in terms of withstanding larger loads and undergoing equivalent deformations without a decrease in stiffness.

Another contribution of this work is a framework to use Kelvin structure for fabrication of objects with spatially-varying elastic properties. We implemented an approach from [Xu et al., 2015] to generate a smooth distribution of Young's moduli within the object from a user-specified deformation behaviour. Having the map, we can derive desired properties for Kelvin cells (sizes) using the models that were adapted by us from material science. To achieve smooth transitions between cells we presented a technique, where we impose the uniform grid structure over the object and warp it in a way to best match target sizes and minimize regions incongruity. We populate the obtained grid with seed,s according to the pattern, that results in the Kelvin cell foam after Voronoi Diagram tesselation. We extract line segments from the diagram's edges and generate slices for fabrication on 3D printer.

Bibliography

Allaire, Gregoire (2002). "Shape Optimization by the Homogenization Method". In: *Springer-Verlag New York*.

Babaee, Sahab et al. (2012). "Mechanical properties of open-cell rhombic dodecahedron cellular structures". In:

Bendsoe, Martin Philip and Ole Sigmund (2004). *Topology Optimization: Theory, Methods and Applications*. en. Springer. ISBN: 9783540429920.

Bickel, Bernd et al. (2010). "Design and Fabrication of Materials with Desired Deformation Behavior". In: *ACM Trans. on Graphics (Proc. SIGGRAPH)* 29.3.

Dunlavy, Daniel M., Tamara G. Kolda, and Evrim Acar (2010). "Poblano v1.0: A Matlab Toolbox for Gradient-Based Optimization". In: SAND2010-1422.

Gibson, L.J. and M.F. Ashby (1989). "Cellular solids: Structure and properties, Oxford: Pergamon Press, ISBN: 0-08-036607-4, 1988, 357 + ix pages". In: *Advances in Polymer Technology* 9.2, pp. 165–166. ISSN: 1098-2329. DOI: 10.1002/adv.1989.060090207. URL: http://dx.doi.org/10.1002/adv.1989.060090207.

Guyan, R.J. (1965). "Reduction of stiffness and mass matrices". In: *AIAA Journal, 3 (2): 380*.

Lévy, Bruno and Yang Liu (2010). "Lp Centroidal Voronoi Tessellation and Its Applications". In: *ACM Trans. Graph.* 29.4, 119:1–119:11. ISSN: 0730-0301. DOI: 10.1145/1778765.1778856. URL: http://doi.acm.org/10.1145/1778765.1778856.

Luxner, Mathias H., Juergen Stampfl, and Heinz E. Pettermann (2007). "Numerical simulations of 3D open cell structures – influence of structural irregularities on elasto-plasticity and deformation localization". In: *International Journal of Solids and Structures* 44.9, pp. 2990 –3003. ISSN: 0020-7683. DOI: https://doi.org/10.1016/j.ijsolstr.2006.08.039. URL: http://www.sciencedirect.com/science/article/pii/S0020768306003465.

Martínez, Jonàs, Jérémie Dumas, and Sylvain Lefebvre (2016). "Procedural Voronoi Foams for Additive Manufacturing". In: *ACM Trans. Graph.* 35.4, 44:1–44:12. ISSN: 0730-0301. DOI: 10.1145/2897824.2925922. URL: http://doi.acm.org/10.1145/2897824.2925922.

Panetta, Julian et al. (2015). "Elastic Textures for Additive Fabrication". In: *ACM Trans. on Graphics - Siggraph 2015* 34.4. Julian Panetta and Quingnan Zhou are Joint first authors, p. 12. URL: http://vcg.isti.cnr.it/Publications/2015/PZMPCZ15.

Schumacher, Christian et al. (2015). "Microstructures to Control Elasticity in 3D Printing". In: *ACM Trans. Graph.* 34.4, 136:1–136:13. ISSN: 0730-0301. DOI: 10.1145/2766926. URL: http://doi.acm.org/10.1145/2766926.

Sullivan, Roy M., Louis J. Ghosn, and Bradley A. Lerch (2008). "A general tetrakaidecahedron model for open-celled foams". In: *International Journal of Solids and Structures* 45.6, pp. 1754 –1765. ISSN: 0020-7683. DOI: https://doi.org/10.1016/j.ijsolstr.2007.10.028. URL: http://www.sciencedirect.com/science/article/pii/S0020768307004465.

Thompson, W.(Lord Kelvin) (1887). "On the division of space with minimum partitional energy". In: *Phil. Mag.* 503.24.

Xu, Hongyi et al. (2015). "Interactive Material Design using Model Reduction". In: *ACM Trans. on Graphics* 34.2.

Zhu, H. X., J. F. Knott, and N. J. Mills (1997). "Analysis of the elastic properties of open-cell foams with tetrakaidecahedral cells". In: *Journal of Mechanics Physics of Solids* 45, p. 319. DOI: 10.1016/S0022-5096(96)00090-7.